

## MULTI-STACKED AND NITROGEN DOPED GRAPHENE LAYERS FOR MICROWAVE HYPERTHERMIA TREATMENT PLANNING WITH LEAST EXPOSURE TIME

SINGLA A.\* , MARWAHA A., MARWAHA S.

ECE Department, Sant Longowal Institute of Engineering & Technology, Longowal  
(Deemed University) Distt. Sangrur, Punjab, India  
\*Corresponding Author: alka.singla274@gmail.com

### Abstract

For treating superficial tumors, patch radiators present a more compact structure and are easy to design. The key requirements for microwave hyperthermia treatment are highly directive and biocompatible antennas with faster penetration rate to minimize the panicking time for patients and negligible detuning of antenna impedance due to frequency dependent tissue properties. In this investigation, graphene-based patch applicator designs have been proposed at a frequency of 915 MHz to obtain a more localized heating pattern. At microwave frequencies, however graphene antenna radiation efficiency is low due to intrinsic dissipative losses. Highly conductive multi-stacked graphene layers and nitrogen doped graphene with sheet resistance value much less than  $10 \Omega/\text{sq}$ . can lead to enhancement in conductivity providing an initial solution for a highly directive non-invasive procedure. For both the approaches simulations have been performed on two different shapes of patch applicators i.e. rectangular patch and twin circular patch. After selecting an optimized distance of 3 mm of the applicator from human phantom, investigations have been done for penetration depth in human body at which maximum value of Specific Absorption Rate (SAR) is achieved. In the first method, rectangular and twin circular graphene-based antenna applicators are proposed by stacking the number of graphene layers from 10 to 50 for producing homogeneous energy deposition and high directivity of 5.66 dB and 6.7 dB respectively. The twin circular graphene patch applicator has been observed to outperform in terms of more localized heating and SAR of 80.9 W/kg at an optimized distance of 3 mm with a depth of 6.2 cm of tumorous site. In the second method, it is further proposed to utilize nitrogen doped graphene utilizing lower resistance values and hence augments in substantially improving the conductivity of applicators. The results show significant improvement in SAR with the value of 114.7 W/kg with nitrogen doped graphene patch applicator for preferred shape of twin circular patch.

Keywords: Microwave hyperthermia, Multi-stacked Graphene Layer (MLG), Nitrogen Doped Graphene (NDG), Rectangular graphene patch, Twin circular graphene patch.

## 1. Introduction

The most often used technology nowadays is microwave hyperthermia for the treatment of cancer [1]. It alludes to the process of transmitting Radio-Frequency (RF) waves into the tumorous tissue to raise the body's temperature from 42 °C to 48 °C. Microwave hyperthermia has received considerably more attention recently because due to its capacity to heat much larger lesions within the constrained treatment period, regulated power distribution [2] and localized heating of tumours [3].

Microstrip antennas that emit electromagnetic radiation into the tissue [4] for frequencies in the Industrial Scientific and Medical (ISM) frequency range at 27 MHz, 434 MHz, 915 MHz, and 2450MHz are the primary methods used to treat superficial cancers using hyperthermia. Microstrip patch antennas have been extensively described in the literature for superficial tumour heating [5-7] due to their compact and planar construction as well as printed circuit board design approaches offering significant design flexibility.

The standard patch antenna applicator, however, has a number of drawbacks, including an inability to target unseen micro metastases and an inability to penetrate the body with sufficient heat. The importance of applicator design is crucial in overcoming these drawbacks. In order to prevent the performance of the radiating antenna from being impacted by frequency dependent and time dependent properties, the applicator should be lightweight, flexible and biocompatible with human tissues. Since graphene nanomaterial is biocompatible with human tissues and also exhibits excellent electrical conductivity, high mechanical strength, and high carrier mobility, it has recently attracted a lot of interest for usage in biomedical applications [8].

Graphene and its derivatives have been thoroughly investigated as nano-carriers for drug delivery in the works [9, 10]. The recently published work [11] incorporate the idea of using graphene material to mitigate backward heating issues in interstitial coaxial antennas for microwave hyperthermia by decreasing surface currents. However, the graphene material has not been well studied for applications as external patch applicator for superficial microwave hyperthermia.

According to Rahman et al. [12], when an antenna is placed close to a body phantom, the dielectric properties of the tissues affect the antenna's performance. In addition, the phantom's capacitive effect adds to the antenna's intrinsic impedance, which raises intrinsic impedance, which further alters impedance matching and reduces antenna performance. This impact is lessened, and mismatch may not happen if the antenna is situated far from the phantom, however at some distances, the antenna may not be able to achieve the desired temperature distribution in the cancerous tissues. Consequently, the study's findings [12] recommend employing a buffer-like layer, a high-capacity bandwidth antenna, and an antenna characterized by intrinsic impedance markedly lower than that of the system impedance, offering a viable solution.

Since graphene is only a moderate conductor at microwave frequencies, graphene-based patch antennas perform poorly in terms of radiation efficiency [13]. Utilizing graphene material for various wireless applications in the terahertz frequencies has been widely explored now these days [14, 15]. However, the detuning effect can be avoided since the surface impedance of graphene with carrier density can be modified to some extent. Few researchers have suggested methods

to enhance the graphene conductivity. Wu et al. in his work [16] demonstrated that multi-stacked graphene layers have potential for achieving reasonable improvement in radiation efficiency in the near field region, by keeping its resistivity in quasi-metallic region. The theoretical study in [16] also suggested that radiation efficiency can be further enhanced by doping or electric biasing. Bala et al. [15] utilized stacked layers of graphene for designing graphene based triangular patch antenna and analysed its performance in terahertz regime.

According to Dai et al. [17] reported the synthesis of nitrogen doping with graphene which has been proven to change the properties of graphene material. Li et al. [18] fabricated nitrogen doped reduced graphene oxide for producing highly conductive graphene films using vacuum filtration method for developing reduced graphene oxide followed by thermal treatment method for nitrogen doping. In the work outlined by reference [19], the process of generating Nitrogen Doped Graphene (NDG) through nitrogen plasma treatment is examined. This method yields exceptionally conductive doped graphene, thereby opening pathways for its utilization in biosensing applications. In this paper, the work is based on utilizing highly conductive graphene sheets as a patch radiator in hyperthermia treatment by following two approaches. First approach is to employ Multi-Layered Graphene (MLG) sheets of low sheet resistance value of  $10 \text{ m}\Omega/\text{sq}$ . and second approach is based on utilizing nitrogen doped graphene layer with specific concentration of nitrogen, carbon and oxygen atoms.

In this study, microwave-frequency rectangular and twin circular microstrip patch antennas employing graphene nanomaterial have been developed. The applicator designs are mounted on a four-layer cylindrical human phantom. The proposed designs have been investigated in terms of distance from the body for optimally positioning the applicators to obtain more localized heating and SAR distribution. COMSOL Multiphysics software, which is based on the Finite Element Method (FEM), was used for the implementation, numerical calculations, and analysis of the designed models.

Figure 1 shows the methods emphasising the important role of graphene for microwave hyperthermia.

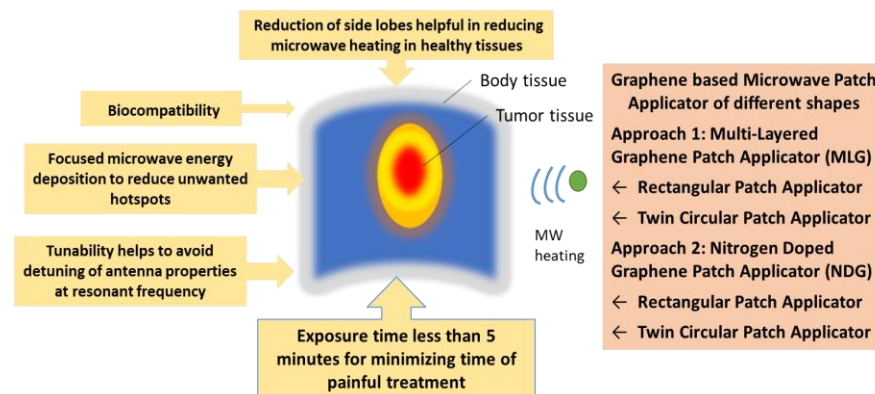


**Fig. 1. Approaches and advantages of graphene patch applicator in microwave hyperthermia treatment.**

The main contribution of the work suggests using highly conductive graphene sheets designed by either multi-stacking graphene layers or by doping of graphene for boosting the characteristics of graphene sheet that enhances the radiation efficiency for specifically targeting the tumors in microwave regime. Nitrogen doping of the graphene material with selected doping concentration can tailor the graphene properties for improved conductivity, enabling it to perform well in the microwave region. The proposed highly conductive graphene sheet applicators fulfil the requirements of high gain and improved radiation efficiency with improved SAR at specific penetration depth.

## 2. Applicator Design

Figure 2 depicts the design of graphene-based rectangular and twin circular patch applicator on FR4 material, having dielectric constant of  $\epsilon_r = 4.5$  and loss tangent of 0.0009. The two circular patches with the same radius depicted in Fig. 2(b), the design is further expanded. Multiple stacks of graphene samples ranging from 10 to 50 were placed on the substrate to create a graphene patch of thickness 't'. The thickness of the graphene stacks can then be estimated as  $t = Nt_l$ , where  $N$  represents the number of stacks ranging from 10 to 50 and  $t_l$  is the thickness of a single graphene layer ( $t_l = 100$  nm). Microstrip line inset feeding of dimensions is utilized with  $50 \Omega$  impedance to match the load providing planar structure to the antenna. An antenna at a resonance frequency of 915 MHz is designed using the patch's proper size. The design parameters for the rectangular patch antenna are assessed using the equations provided in [20], and the values are given in Table 1.

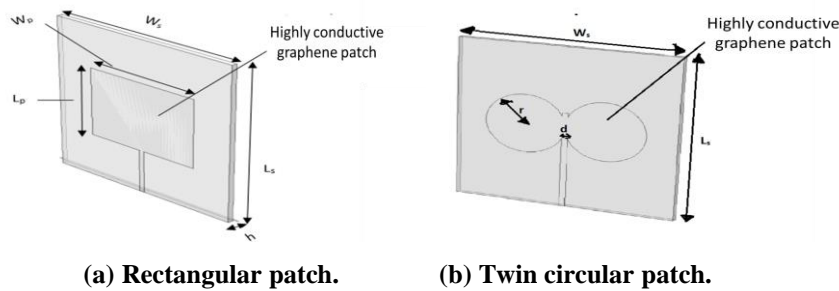


Fig. 2. Graphene-based patch antenna designs.

Table 1. Design parameters of graphene-based patch antenna.

Parameter	Design values
Length of substrate, $L_s$	90 mm
Width of substrate, $W_s$	110 mm
Thickness of substrate, $h$	1.6 mm
Relative permittivity of dielectric substrate, $\epsilon_r$	4.5
Length of rectangular patch, $L_p$	58 mm
Width of rectangular patch, $W_p$	76 mm
Resonant frequency, $f$	915 MHz
Effective radius of twin circular annular ring, $r_a$	14 mm
Distance between two annular rings, $d$	3 mm
Length of feed, $L_f$	14 mm
Width of feed, $W_f$	3 mm
Thickness of monolayer graphene patch	100 nm

## 2.1. Properties of Graphene

Single layer of graphene with very negligible thickness (1-atom thick) for a conducting patch leads to a 2-D geometry. But at microwave frequencies graphene behaves as a poor conductor so to improve the radiation efficiency multilayer graphene film with high conductivity has been designed with total thickness 't' that substantially reduces propagation currents in healthy tissues for effectively delivering the heat to targeted tissues. Bozzi et al. [21] gives the expression for conductivity of graphene can be expressed by Kubo's formula approximated as an interband contribution given in Eq. (1).

$$\sigma_{intra}(\omega) = \frac{2e^2 k_B T}{\pi \hbar^2} \ln \left[ 2 \cosh \left[ \frac{\mu_c}{2k_B T} \right] \right] \frac{j}{\omega + j\tau^{-1}} \quad (1)$$

where  $\tau = 10^{-13}$  s is the relaxation time,  $\mu_c$  is the chemical potential,  $k_B$  is the Boltzmann's constant,  $\hbar$  is the reduced Planck's constant i.e.  $\hbar = \frac{h}{2\pi}$ ,  $T$  is room temperature in Kelvins,  $\omega$  is the radian frequency and  $e$  is the charge of electron. The surface impedance of graphene sheet is  $Z_s = \frac{1}{\sigma(\omega)}$ . The chemical potential can significantly vary the conductivity and surface impedance. In graphene, the chemical potential is related to the carrier density  $n$  ( $m^{-2}$ ) from the following equation Eq. (2).

$$n = \frac{2}{\pi (\hbar v_f)^2} \int_0^\infty \varepsilon [f_d(\varepsilon - \mu_c) - f_d(\varepsilon + \mu_c)] d\varepsilon \cong \frac{(\mu_c / (\hbar v_f)^2)^2}{\pi} \quad (2)$$

The conductivity of graphene can also be enhanced by doping of graphene and the conductivity of doped material is given as in Eq. (3).

$$\sigma_D = n_D q \mu_D \quad (3)$$

where  $q$  is the electron charge (C),  $n_D$  ( $m^{-3}$ ) and  $\mu_D$  ( $m^2/Vs$ ) are the free carrier density and mobility of doped semiconductor, respectively. Wu et al. [16] suggested that for sheet resistance  $R_s < 10 \Omega/sq.$  (in quasi-metallic region), radiation gain of a graphene patch can be larger than 0 dB and it continues to increase with decreasing value of sheet resistance. The author also observed that in lossy dielectric region i.e.,  $R_s > 10 \Omega/sq.$  graphene acts as absorbing agent in spite of increasing the number of layers from 1 layer to 5 layers. The sheet resistance values are measured by four-point probe method. Based on these issues related to graphene material, MLG sheet with high conductivity of  $1.13 \times 10^6$  S/m and low sheet resistance of 10 m $\Omega/sq.$  has been utilized in the proposed applicator design. The authors further showed that for low sheet resistance ( $R_s < 10 \Omega/sq.$ ) in the quasi-metallic region the peak gain of the graphene patch can be increased to an acceptable level ( $> 0$  dBi), by either doping of graphene layer or by electrical biasing [16]. Among the numerous potential dopants, nitrogen is an excellent element for the chemical doping of carbon materials because it is of comparable atomic size and contains five valence electrons available to form strong valence bonds with carbon atoms.

Wang et al. [19] fabricated the nitrogen doped graphene by using nitrogen plasma treatment for 40 minutes in the chamber and the power of 100 W. The percentage of doping graphene is analyzed by X-ray photoelectron spectroscopy. The authors considered nitrogen concentration of 1.35% with carbon and oxygen

atoms of concentration 71.09 % and 28.05 % respectively, with surface area of  $1 \text{ m}^2$  for improved radiation efficiency and minimizing propagation surface waves for suppressing the undesirable heating.

The applicator having MLG is therefore properly designed to match the input impedance of  $50 \Omega$  and simulated for measuring microwave scattering parameters. The performance of conventional patch antennas using copper conductors is highly affected by the frequency dependent dielectric properties of the human tissues [22]. Due to the biocompatibility of graphene material, the designed graphene-based patch antenna undergoes minimum variations. Further the reconfigurability of graphene-based patch antenna can substantially overcome any undesirable detuning effects resulting from frequency shifts.

The return loss plot for both rectangular patch applicator and twin circular patch applicator with maximum 50 stacks of graphene layer and Single Layer Graphene (SLG) are presented in Fig. 3. It is revealed from the figure that for a single graphene layer with no stacks, return loss of -22 dB and -15 dB is achieved for twin circular patch applicator and rectangular patch applicator, respectively. With increased number of graphene layers improved return loss performance is achieved in coherence with the reported literature [16]. Maximum return loss value of -32 dB and -24.3 dB is achieved with 50 stacks of graphene layers for twin circular patch applicator and rectangular patch applicator, respectively.

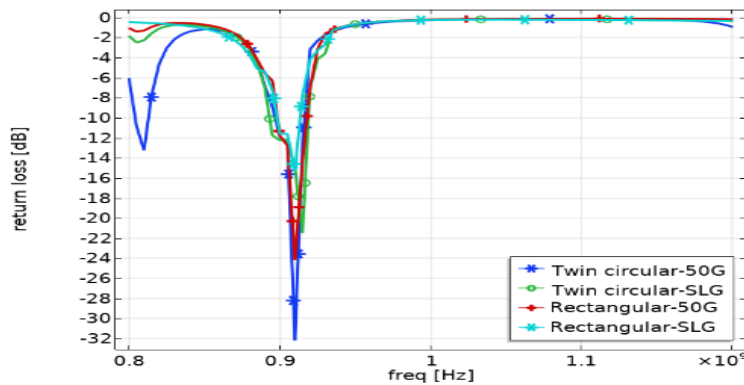


**Fig. 3. Return loss characteristics of SLG and MLG of graphene-based patch applicators.**

Further for analysing the effect of human body phantom on antenna performance, the simulated return loss graph for 50 stacks of graphene layer for twin circular patch applicator with and without the human body phantom is shown in Fig. 4. It can be visualized from the figure that the resonant frequency is shifted slightly in the presence of human body phantom. The dimensions of the configurations are selected accordingly, and models are designed for operation at 915 MHz with body phantom.

The conductivity of graphene can be further enhanced by doping of graphene material with nitrogen [18]. For numerical modeling of second configuration, the characterization of NDG is performed in accordance with the chemical composition of nitrogen doped graphene as fabricated in [19]. The electrical and chemical

properties of NDG used for the simulation of nitrogen doped graphene patch applicators include electrical conductivity of  $8.33 \times 10^5$  S/m, mobility of  $450 \text{ cm}^2/\text{V/s}$  and band gap energy of 0.2 eV.

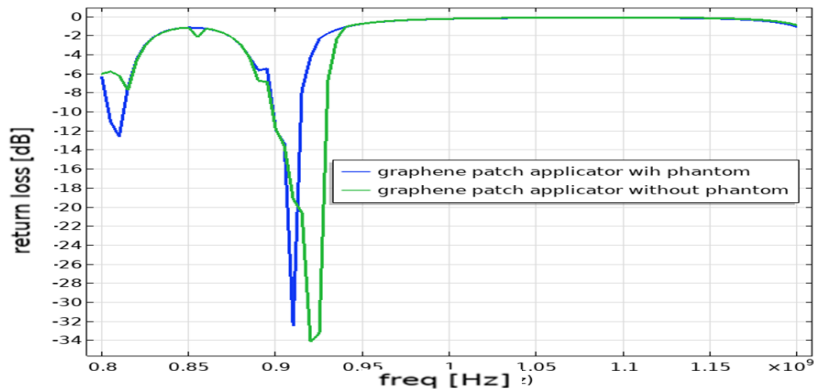


**Fig. 4. Return loss characteristics for 50 stacks of graphene-based twin circular patch applicator with or without body phantom.**

The appropriate selection of properties of graphene material enforces the graphene-based antenna to perform as a radiating patch conductor at microwave frequencies. The simulated models of NDG based patch applicators are assigned requisite materials and boundary conditions and subsequently processed for result analysis. The return loss curves plotted in Fig. 5 for rectangular and twin circular patch applicators with doped graphene layers show that reasonably good return loss value below -30 dB is obtained for both the designs with a maximum dip of -33 dB for twin circular patch applicator. The resonant frequency for twin circular patch applicator is 915 MHz whereas minor variation can be seen for rectangular patch applicator. The dimensions for two shapes of applicators are kept constant for analysing the MLG and NDG based applicators. Due to difference in EM properties of MLG and NDG, the rectangular patch applicator resonates at a slightly deviated frequency of 910 MHz.

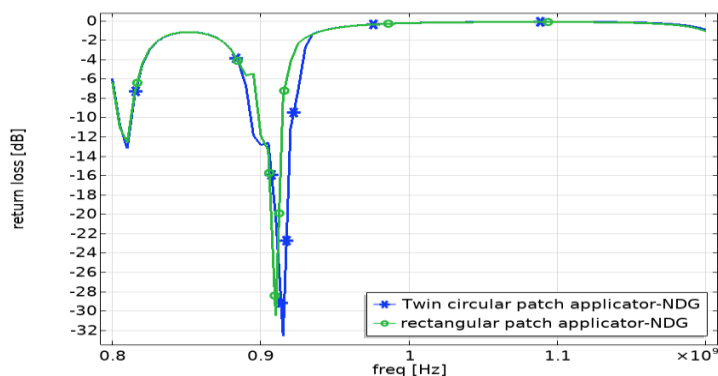


**Fig. 5. Return loss characteristics for nitrogen doped graphene-based patch applicators.**

## 2.2. Human body phantom

The design and performance of antennas for hyperthermia involves numerical solution of the EM and thermal problems that is the solution of Maxwell equations and the Bioheat Transfer Equation (BHE) respectively [23]. The human phantom model is mounted on microstrip patch antenna at some optimized distance by introducing an air gap in-between in order to evaluate the temperature distribution of human organic tissue. The organic tissue is assumed to be cylindrical with 4-layers of muscle phantom i.e. skin, fat, muscle and bone. Thermal model comprises of four cylinders having radius  $d_{skin}$  (100 mm),  $d_{fat}$  (90 mm),  $d_{muscle}$  (70 mm) and  $d_{bone}$  (40 mm) (perpendicular to the feeder axis) forming the different layers of the tissues and the tumor is modelled as truncated cylinder in the skin layer as depicted in Fig. 6. Thickness of the truncated cylinder is same as the thickness of skin layer. The electromagnetic and thermal properties of these elements are presented in Table 2.

**Table 2. Dielectric properties of human tissues [24].**

Tissue	Relative permeability ( $\mu_r$ )	Relative permittivity ( $\epsilon_r$ )	Conductivity ( $\sigma$ ) (S/m)	Density ( $\rho$ ) ( $\text{kg/m}^3$ )	Specific heat ( $C_p$ ) (J/kg.K)
Skin	1	37	0.70	1100	3400
Fat	1	14.6	0.33	920	2500
Muscle	1	61	1.31	1041	3500
Bone	1	22.5	0.17	1500	1300
Tumor	1	59	0.65	1050	3639

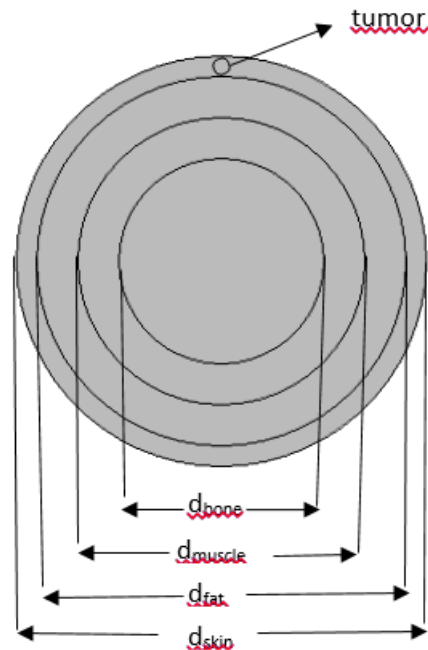
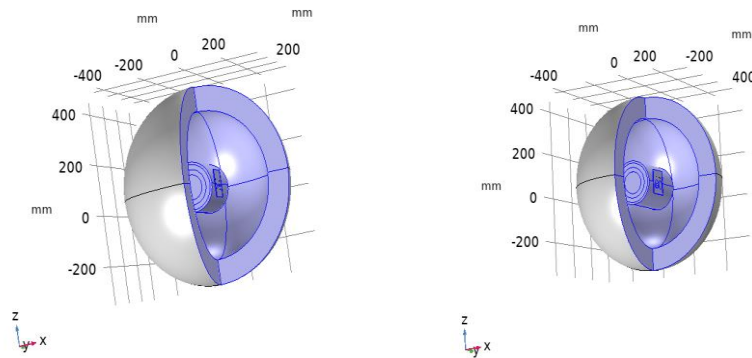


**Fig. 6. Geometry of organic tissue.**

Figure 7 shows the COMSOL modeling of whole geometry for both patch applicators with 4-layer human body phantom surrounded by Perfectly Matched Layer (PML). In order to predict the induced fields into the target tissues for coupled EM problems, the numerical simulation of bio-electromagnetic problem is done in RF module and heat transfer module of COMSOL using Multiphysics capability of the software to solve coupled problem [25]. The entire geometry is built in spherical domain of radius 200 mm and layer thickness of 50 mm as PML so as to absorb outward radiations from the patch antenna. The body phantom is placed in x-direction at a distance of 3 mm from the antenna applicator.



(a) Rectangular patch.

(b) Twin circular patch.

Fig. 7. Patch applicator models with body phantom.

### 3. Results and Discussions

The performance of the patch applicator designs for hyperthermia treatment is evaluated in terms of SAR distribution and temperature distribution by placing the antenna at varying distance from human phantom. All the simulation results are presented for multi-stacked graphene layer in Section 3.1 followed by simulation results of nitrogen doped graphene in Section 3.2.

#### 3.1. Multi-stacked graphene layer simulation results

For graphene-based patch antenna applicator, at operating frequency of 915 MHz, the antenna is poorly matched making it a poor conductor. However, for efficiently delivering heat to targeted tissues highly conductive graphene film with multi-stacks have been used. The model is created using adaptive mesh refinement strategies that permits extra fine mesh refinement iteratively in regions where high accuracy is needed. The better mesh refinement algorithms are also helpful for modeling thin graphene layers which demands for efficiently selecting the mesh density. For graphene antenna, shape of the structure is expected to influence the radiation characteristics. The edge shape of the defined structure attains either zigzag or armchair arrangement possessing different electronic properties hence leading to different performance [26]. Resonance is also an important characteristic of an antenna when the antenna input matches the impedance of source. The radiation patterns of rectangular patch applicator and twin circular patch applicators are depicted in Figs. 8(a) and (b) respectively at frequency of 915 MHz. The antenna radiation characteristics are obtained for  $\theta$  angle of  $110^\circ$  and  $\Phi$  angle of

162° directing completely towards the body phantom. It is noticeable from these plots that much enhanced gain of more than 6.5 dB is achieved for 50 G twin circular patch applicator as compared to rectangular patch applicator. It is depicted that antenna gain is improved for increased stacking layers of graphene on account of increased conductivity of graphene [16].

For maximum energy deposition in the focused area highly directive antennas are desired. Figure 8 shows the radiation pattern plots demonstrating high directivity of 6.7 dB and 5.6 dB for twin circular and rectangular patch applicators, respectively. Graphene patch applicator causes increased radiation in the forward direction and also provides better shielding in the reverse direction. Figure 9 depicts the polar plot gain curves for both the applicators achieving a beam width of 46°.

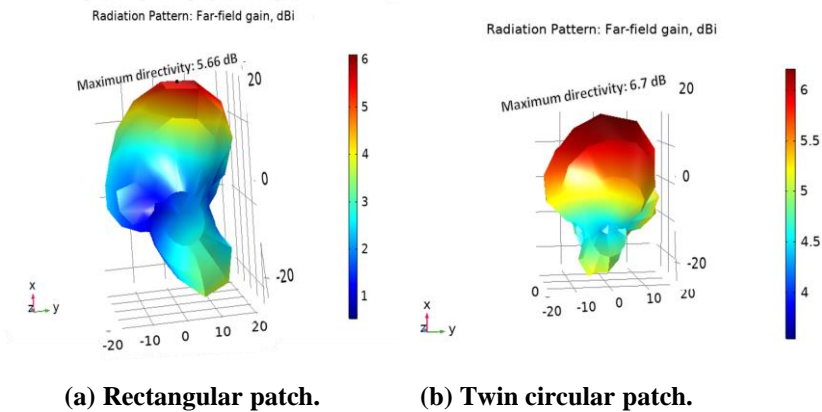


**Fig. 8. Radiation pattern characteristics of MLG.**

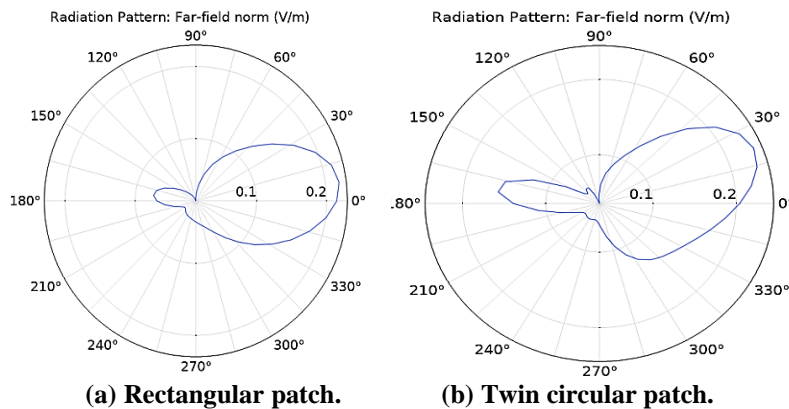


**Fig. 9. Polar plot gain of MLG.**

SAR distribution plots discussed in this section show that improved SAR is obtained in the tumorous cells and surface currents are lowered in healthy tissues. In order to obtain highly localized value of SAR, distance of patch from the body phantom is varied to find the optimized distance. The temperature distribution plots for both configurations of graphene-based patch applicator with no stack of graphene layer and maximum 50 stacks of graphene layer at a distance ( $d_{min}$ ) of 0

mm and 3 mm from the body phantom are shown in Figs. 10 and 11, respectively. For rectangular patch applicator temperature reaches to 317°K ( $\approx 43.85^\circ\text{C}$ ) at 0 mm distance which is within the limits for hyperthermia treatment the heating pattern is however not localized as shown in Fig. 10(c). It can be observed from Fig. 11(c) that twin circular patch applicator obtains a maximum temperature of 321.7°K ( $\approx 48.7^\circ\text{C}$ ) and more uniform heating of cylindrical tissues with high value of SAR as 80.9 W/kg for maximum of 50 graphene stacks when the antenna is just placed near the body i.e. at 0 mm distance. However, to avoid any superfluous damage to human skin, the antenna must be placed at some distance from the body surface. Hence the temperature distribution and SAR patterns are further determined by placing the applicators at sufficient distance ( $d_{min}$ ) of 3 mm.

To find optimized the distance of the patch applicator from the human phantom, the performance is determined with distance variations ( $d_{min}$ ) from 0 to 20 mm with a step size of 3 mm for multiple stacks of graphene layer ranging 10 to 50. Twin circular patch applicator outperforms the rectangular patch applicators can be visualized from the SAR and temperature distribution plots shown in Figs. 12 and 13, respectively. It is evident that patch applicator placed at an optimum distance of 3 mm results in the temperature as 319.9°K ( $\approx 46.75^\circ\text{C}$ ) for twin circular applicator with more localized heating. With further increase in distance of the applicator from body the SAR value gradually declines with a value of 62 W/kg at distance of 4 mm. The reduced SAR would noticeably cause limited heating of tumor tissue. From Table 3 it can be seen that at distance of 10 mm, the temperature drops down to 315°K ( $\approx 41.85^\circ\text{C}$ ) which is lower than the temperature requirements for hyperthermia.

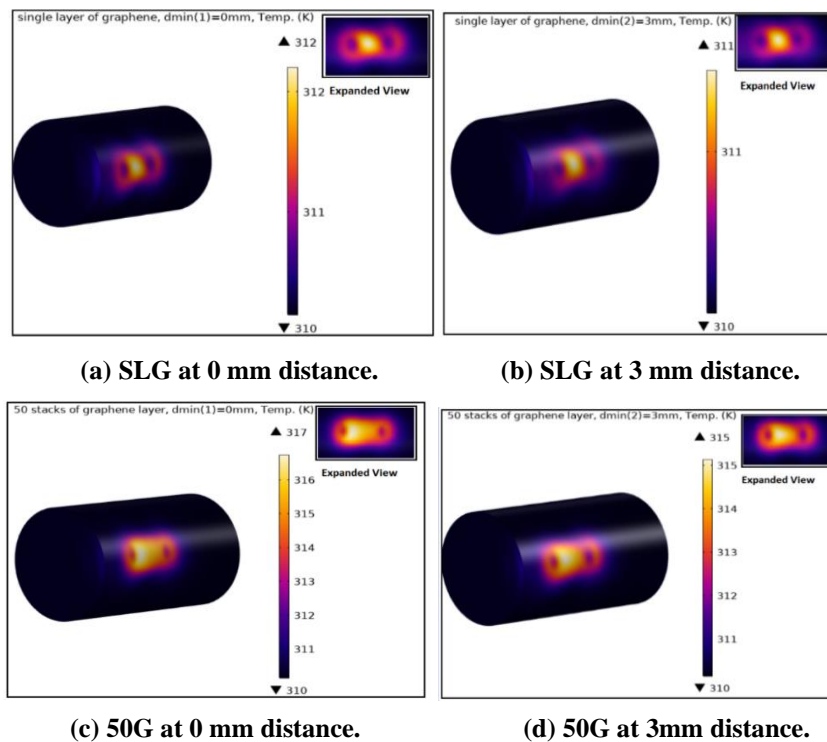


Fig. 10. Temperature distribution plots for rectangular patch applicator.

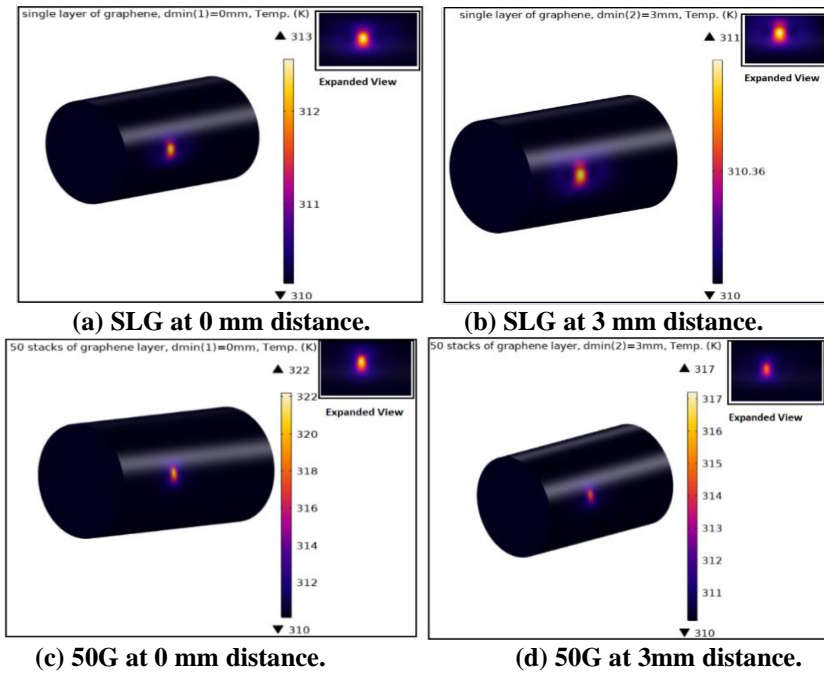


Fig. 11. Temperature distribution plots for twin circular patch applicator.

Table 3. SAR and temperature distribution values for varying distance of twin circular patch applicator.

$d_{min}$ (mm)	50 stacks		40 stacks		30 stacks		20 stacks		10 stacks		No. stacks	
	SAR (W/kg)	T (°K)	SAR (W/kg)	T (°K)	SAR (W/kg)	T (°K)	SAR (W/kg)	T (°K)	SAR (W/kg)	T (°K)	SAR (W/kg)	T (°K)
0	80.9	322.2	60.6	320.8	50.6	319.7	40.6	316.7	38.1	315.7	28.1	313.3
3	64.2	319.9	49.7	318.3	44.7	317.3	35.7	315.3	32.4	314.3	20.4	311.3
6	57.5	318.5	43.6	316.0	40.6	315.9	24.6	314.9	20.1	313.9	15.1	310.9
9	50.3	317.4	35.7	314.9	18.7	314.2	17.7	314.2	14.9	312.2	12.9	310.7
12	44.1	315.8	25.6	313.7	17.6	314	16.6	313.3	10.9	311.3	11.6	310.4
15	28.4	314.5	18.7	312.0	9.7	313	9.7	312.1	6.7	311.1	5.7	310.1
18	13.7	313.4	5.0	311.4	3.0	311	2.0	311	1.0	310	1.0	310

### 3.2. Nitrogen doped graphene layer simulation results

Nitrogen doped graphene patch conductor further enhances the performance. The radiation pattern plot for highly directive nitrogen doped applicator is shown in Fig. 14 for both the applicator designs. Significant improvement in antenna gain is achieved by doping of nitrogen in graphene which effectively varies the electrical properties causing increased conductivity [19]. A maximum gain of 7.4 dB and 8 dB is achieved for nitrogen doped rectangular and twin circular applicator, respectively. Polar gain plots are depicted in Fig. 15 clearly depicts a highly directive radiation pattern with maximum radiation efficiency and reduced side lobes.

Figure 16 plots temperature distribution for both the applicators exhibiting maximum temperature of about 320°K apparently. However, twin circular patch applicator provides more uniform heating. Also, the microwave energy deposited inside phantom have significant penetration depth. Thus, SAR distribution plot

with respect to penetration depth inside the muscle phantom are depicted in Fig. 17. The SAR distribution plots apparently demonstrate highly localized heating for nitrogen doped graphene for both applicators. Twin circular patch applicator with nitrogen doped graphene has maximum SAR of 113.1 W/kg and temperature of 319.7°K at penetration depth of 6.1 cm inside the phantom and rectangular patch applicator with nitrogen doped graphene has maximum SAR of 100.9 W/kg and temperature of 319.1°K at penetration depth of 5.5 cm.

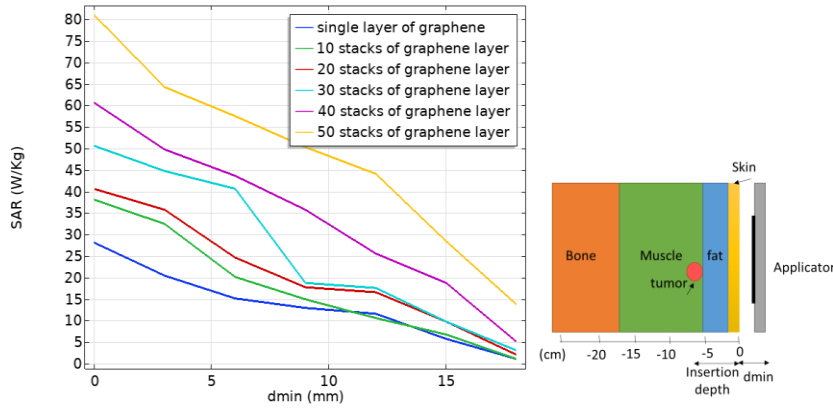


Fig. 12. SAR vs optimized distance plot for twin circular patch applicator.

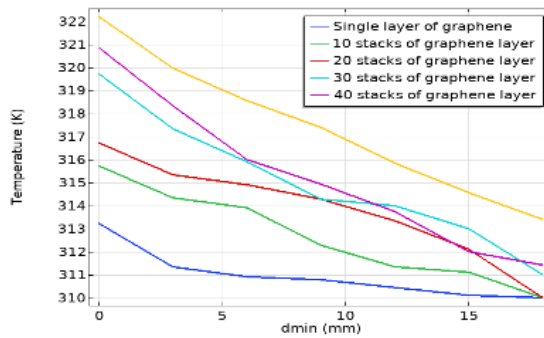
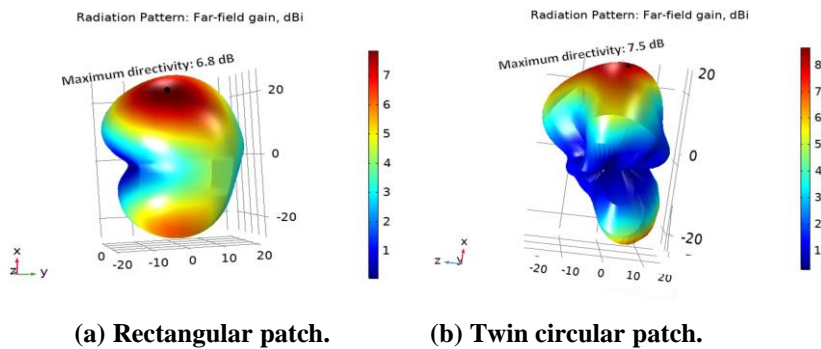
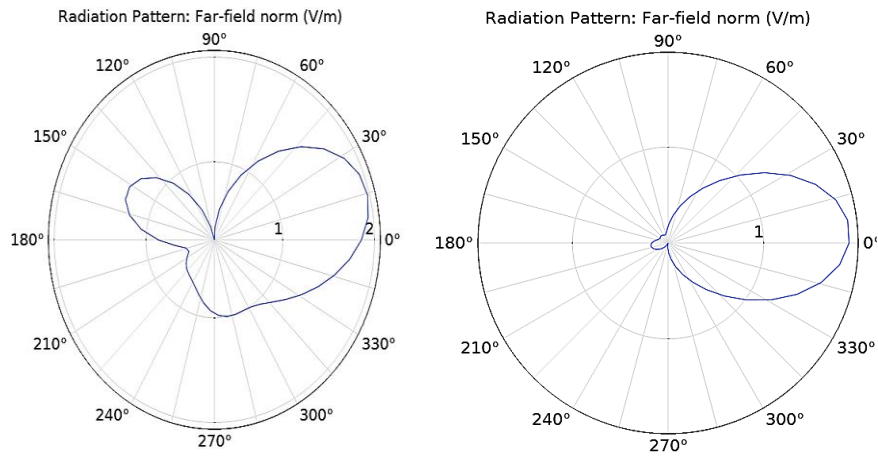


Fig. 13. Temperature distribution vs optimized distance plot for twin circular patch applicator.



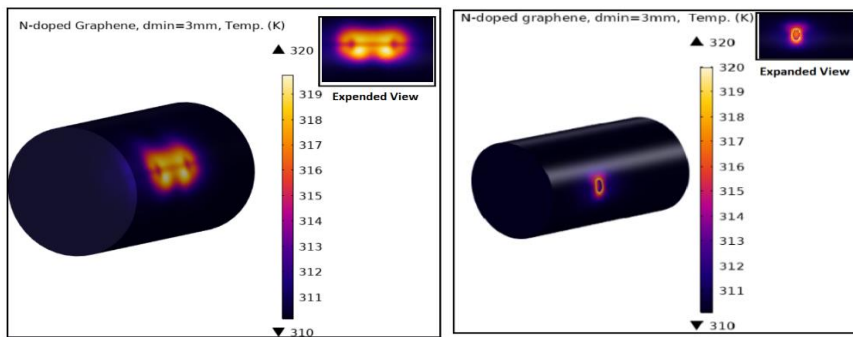
(a) Rectangular patch. (b) Twin circular patch.

Fig. 14. Radiation pattern characteristics of DG.



(a) Rectangular patch. (b) Twin circular patch.

Fig. 15. Polar plot gain of NDG.



(a) Rectangular patch. (b) Twin circular patch.

Fig. 16. Temperature distribution plot for NDG at 3 mm distance.

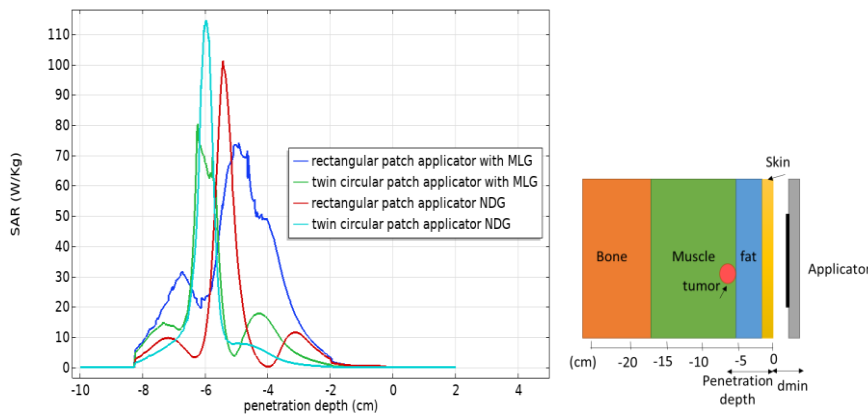


Fig. 17. SAR versus penetration depth plot

The SAR values for two approaches are compared in Table 4 and determined for 50 stacks of graphene patch applicators and nitrogen doped graphene at different values of penetration depth considering optimized distance of 3 mm. For effective transmission of EM waves into biological tissues, nitrogen doping of graphene apparently provides a better choice. The temperature variation is also in the permissible limits for hyperthermia treatment.

**Table 4. SAR values at different penetration depths for both applicators.**

Penetration depth	SAR values (W/kg)			
	Multi-stack Graphene Rectangular patch applicator (MLG)	Multi-stack Graphene Twin circular patch applicator (MLG)	Nitrogen Doped Graphene Rectangular patch applicator (NDG)	Nitrogen Doped Graphene Twin circular patch applicator (NDG)
0 cm	0.3	0.1	0.2	0.01
1 cm	1.21	0.21	0.5	0.05
2 cm	3.7	0.8	3.1	0.26
3 cm	15.2	4.1	11.3	1.13
4 cm	48.7	16.69	1.0	4.9
5 cm	73.3	4.0	49.0	8.4
6 cm	22.3	67.6	100.1	113.1
7 cm	26.3	13.6	9.4	8.5
8 cm	8.5	7.3	4.2	2.5
9 cm	2.0	4.4	3.0	1.6
10 cm	1.0	1.7	1.9	2.3

Further treatment time is investigated for the preferred shape of twin circular patch applicator using both the approaches of multi-stacking and nitrogen doping. Figure 18 shows the variation of temperature in °C inside the tumor tissues with respect to time. It can be visualized from the figure that maximum temperature is achieved within 5 minutes of treatment time. The maximum temperature attained for nitrogen doped graphene-based twin circular patch applicator is 47°C in 300 seconds. Lesser rise in temperature is however observed for multi-stacked graphene-based twin circular patch applicator within same duration of time.

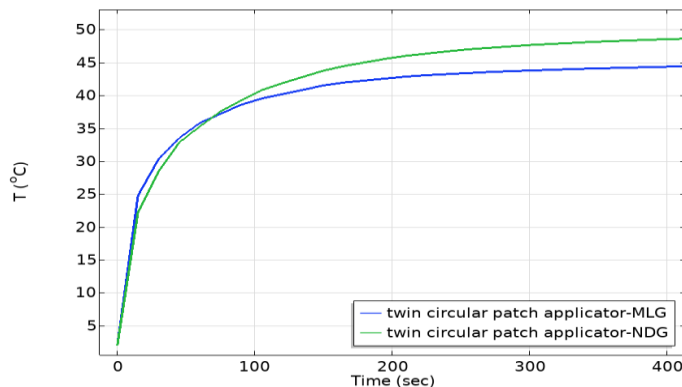


**Fig. 18. Temperature variation with respect to time for twin circular patch applicator using both approaches.**

The possibility of improved performance in patch applicator can be owing to the zigzag arrangement at the edges of graphene patch as reported in [26]. The zigzag structure possesses higher input impedances which could cause effective suppression of surface currents for reduced backward heating. The number of stacks of graphene can also be increased beyond 50 for further improving radiation efficiency but it would increase the temperature also to a value much higher than 321.2°K ( $\approx 48^\circ\text{C}$ ) which is not desirable for the hyperthermia application. Hence all the evaluations have been performed for applicators with maximum 50 stacks of graphene at distance of 3 mm.

The results obtained from the designed antenna applicator with multiple graphene stacks and nitrogen doped graphene can therefore be used as comparative measure for optimally selecting the graphene-based patch applicator based on more localized heating patterns.

Table 5 shows comparison of current study of using nanomaterial with earlier reported research for hyperthermia treatment of superficial tumors. Gaffoglio et al. [27] proposed a strategy to improve the focussed temperature and SAR distribution on the target. SAR value of 55.47 W/kg is obtained with the optimization algorithm. Other studies on focussed heating have been conducted using multiple antenna arrays designed mainly for treatment in the pelvic region [28, 29]. Fiser et al. [30] proposed an array applicator design of octagonal shape patch elements operating at frequency 434 MHz. The authors have demonstrated that SAR contours are enclosed by 25%, 50 % and 75% of effective area for increasing the number of elements from 4, 6 and 8. High input power of 50 W is required for heating tumor tissue with 12 °C rise in temperature and also penetration depth is restricted to 2.7 mm.

**Table 5. Comparison of results from literature.**

Applicator Design	Frequency	Dimensions	SAR value (W/kg)	Rise in temp. (°C)	Return loss (dB)	Applied input power	Exposure time (minutes)	Reference
Rectangular patch antenna	2.45 (GHz)	57 × 49 mm <sup>2</sup>	2.34	--	-37	10 W	177	[4]
Phased array applicator	435 (MHz)	37.6 × 10 <sup>4</sup> mm <sup>2</sup>	55.47	8	--	--	--	[27]
Coherent phased array	0.5-2 (GHz)	7.8 × 10 <sup>3</sup> mm <sup>2</sup>	70	--	--	--	--	[28]
Time reversal-based patch array applicator	500-900 (MHz)	61.5 × 10 <sup>3</sup> mm <sup>2</sup>	40	--	-20	30 W	--	[29]
Planar antenna array applicator	434 (MHz)	100 × 100 mm <sup>2</sup>	--	12	-10	50 W	3	[30]
Microstrip patch antenna	2.45 (GHz)	38.57 × 46.88 mm <sup>2</sup>	14.8	8	--	1 W	30.78	[31]
Slotted circular patch antenna	2.45 (GHz)	100 mm <sup>2</sup>	--	11.4	-24	2 W	10	[32]
Graphene-based rectangular patch antenna	915 (MHz)	110 × 90 mm <sup>2</sup>	100.1	10	-30	10 W	5	Proposed research
Graphene-based twin circular patch antenna	915 (MHz)	110 × 90 mm <sup>2</sup>	113.1	11	-32	10 W	5	Proposed research

Further, the latest available literature [4, 31] propose to design single element planar microstrip patch applicator for treatment of tumor operating at higher resonant frequency of 2.45 GHz. Though low microwave input power is utilized but the main issues are that very low SAR value is obtained, and exposure time is also too large causing much discomfort to patients. The literature cited in the table shows that for the treatment of superficial tumorous cells, antenna array applicators are invariably being used for localizing and targeted heat lesion.

The arrays lead to bulky design and single patch applicator also fails to provide good heat absorption in less treatment time. Keeping in view of the dimensions and optimized applied input power restricted to 10 W, the proposed graphene-based single element patch applicator offers sufficient rise in temperature and much improvement in SAR values with distribution at tumour sites only to effectively kill the tumor tissues without effecting healthy tissues. The applicator designs utilizing graphene nanomaterial achieve SAR of 100.1 W/kg and 113.1 W/kg for the rectangular patch antenna and twin circular patch antenna respectively.

#### **4. Conclusions**

Superficial hyperthermia treatment demands a highly localized heating pattern with minimum exposure time of the human tissues. Two alternate approaches are suggested to design the antenna applicators for achieving the desired performance. The biocompatible graphene material is employed to design multi-stacked, and nitrogen doped graphene-based rectangular and twin circular patch applicators to compensate for reduced radiation efficiency on account of poor conductivity of graphene at microwave frequencies.

The applicators are investigated for localized energy deposition in terms of SAR values for the distance varying from 0 mm to 20 mm. The maximum directivity of 5.66 dB and 6.7 dB is achieved for multi-stacked rectangular and twin circular patch applicator respectively whereas considerably high directivity of 7.97 dB and 8.02 dB is achieved for nitrogen doped rectangular and twin circular patch applicator respectively which is helpful in improving the radiation efficiency at target site and reducing unwanted microwave heating of healthy tissues.

Improvement in results is visualized for multiple stacking of graphene layers as evidenced from SAR and temperature distribution plots. It has been demonstrated that twin circular patch applicator with 50 stacks of graphene attains localized heating by placing an antenna at distance of 3 mm.

However more satisfying results were obtained with nitrogen doped graphene for twin circular patch as compared to multi-layered graphene patch applicators. Much higher SAR value of 114.7 W/kg is achieved with low sheet resistance value of 10  $\Omega$ /sq. owing to sheet resistivity property of graphene at microwave frequencies.

The maximum temperature of 321.9°K (within acceptable limit of hyperthermia treatment) is reached with nitrogen doped graphene-based twin circular patch applicator. The heat can be effectively transferred into the biological tissues with least exposure time of 10 minutes using both approaches hence providing better solutions for mitigating backward heating problem for successful removal of superficial tumors.

## Acknowledgement

This work is supported by the DST FIST-2018 Project (Reference No. SR/ET-I/2018/157).

### Nomenclatures

$C_p$	Specific heat of tissue, J/kg.K
$d$	Distance between twin circular annular ring, mm
$d_{bone}$	Diameter of bone layer, mm
$d_{fat}$	Diameter of fat layer, mm
$d_{min}$	Minimum distance of applicator from phantom, mm
$d_{muscle}$	Diameter of muscle layer, mm
$d_{skin}$	Diameter of skin layer, mm
$f$	Resonant frequency, MHz
$h$	Height of substrate, mm
$k_B$	Boltzmann constant, eV
$L_f$	Length of feed, mm
$L_p$	Length of patch, mm
$L_s$	Length of substrate, mm
$N$	Number of stacks
$n$	Carrier density, $m^{-3}$
$n_d$	Free charge carrier density of doped semiconductor, $m^{-3}$
$R_s$	Sheet resistance of graphene, $\Omega/sq.$
$r_d$	Effective radius of twin circular patch, mm
$t$	Thickness of graphene patch layer, nm
$W_f$	Width of feed, mm
$W_p$	Width of patch, mm
$W_s$	Width of substrate, mm
$Z_s$	Surface impedance of graphene, $\Omega$

### Greek Symbols

$\mu_D$	Mobility of doped semiconductor, $m^2/Vs$
$\mu_c$	Chemical potential, eV
$\epsilon_r$	Relative permittivity of dielectric substrate
$\epsilon_r$	Relative permittivity of tissues
$\mu_r$	Relative permeability of tissues
$\rho$	Density of Tissues, $kg/m^3$
$\tau$	Relaxation time, s
$\hbar$	Reduced Planck constant, eVs
$\sigma$	Conductivity of Tissues, S/m
$\omega$	Radian frequency, rad/s

### Abbreviations

BHE	Bioheat Transfer Equation
FEM	Finite Element Method
ISM	Industrial Scientific Medical Band
MLG	Multi Layered Graphene
NDG	Nitrogen Doped Graphene

PML	Perfectly Matched Layer
SAR	Specific Absorption Rate
SLG	Single Layer Graphene

## References

1. Altintas, G.; Akduman, I.; Janjic, A.; and Yilmaz, T. (2021). A novel approach on microwave hyperthermia. *Diagnostics*, 11(3), 493.
2. Kandala, S.K.; Liapi, E.; Whitcomb, L.L.; Attaluri, A.; and Ivkov, R. (2019). Temperature-controlled power modulation compensates for heterogeneous nanoparticle distributions: a computational optimization analysis for magnetic hyperthermia. *International Journal of Hyperthermia*, 36(1), 115-129.
3. Kok, H.P.; Cressman, E.N.; Ceelen, W.; Brace, C.L.; Ivkov, R.; Grüll, H.; Ter Haar, G.; Wust, P.; and Crezee, J. (2020). Heating technology for malignant tumors: a review. *International Journal of Hyperthermia*, 37(1), 711-741.
4. Hassan, M.M.; Lias, K.; Buniyamin, N.; Naimullah, B.S.S.; and Jobli, A.T. (2021). SAR performance of rectangular microstrip antenna for breast cancer hyperthermia treatment with different period of treatment procedure. *Proceedings of the International Conference on Biomedical Engineering (ICoBE)*, UniMAP, Malaysia, 2071(1), 012048.
5. Chakaravarthi, G.; and Arunachalam, K. (2015). Design and characterization of miniaturized cavity- backed patch antenna for microwave hyperthermia. *International Journal of Hyperthermia*, 31 (7), 737-748.
6. Curto, S.; McEvoy, P.; Bao, X; and Ammann, M.J. (2011). Compact patch antenna for electromagnetic interaction with human tissue at 434 MHz. *IEEE Transactions on Antennas and Propagation*, 57(9), 2564-2571.
7. Zafar, T.; Zafar, J.; and Zafar, H. (2014). Development and microwave analysis of slot antennas for localized hyperthermia treatment of hepatocellular liver tumor. *Australasian Physical and Engineering Sciences in Medicine*, 4, 673-679
8. Li, J.; Zeng, H.; Zeng, Z.; Zeng, Y.; and Xie, T. (2021). Promising graphene-based nanomaterials and their biomedical applications and potential risks: a comprehensive review. *ACS Biomaterials Science and Engineering*, 7(12), 5363-5396.
9. Wilson, A.J.; Rahman, M.; Kosmas, P.; and Thanou, M. (2021). Nanomaterials responding to microwaves: an emerging field for imaging and therapy. *Nanoscale Advances*, 3(12), 3417-3429.
10. Chang, D.; Lim, M.; Goos, J.A.; Qiao, R.; Ng, Y.Y.; Mansfeld, F.M.; Ackson, M.; Davis, T.P.; and Kavallaris, M. (2018). Biologically targeted magnetic hyperthermia: Potential and limitations. *Frontiers in Pharmacology*, 9, 831.
11. Uzman, B.; Yilmaz, A.; Acikgoz, H.; and Mittra, R. (2021). Graphene-based microwave coaxial antenna for microwave ablation: thermal analysis. *International Journal of Microwave and Wireless Technologies*, 13(5), 497-505.
12. Rahman, N.H.; Yamada, Y.; and Amin Nordin, M.S. (2019). Analysis on the effects of the human body on the performance of electro-textile antennas for wearable monitoring and tracking application. *Materials*, 12(10), 1636.
13. Perruisseau-carrier, J.; Tamagnone, M.; Gomez-Diaz, J.S.; and Carrasco, E. (2013). Graphene antennas: can integration and reconfigurability compensate

- for the loss. *Proceedings of the 2013 European Microwave Conference*, Nuremberg, Germany, 369-372.
14. Bala, R.; and Marwaha, A. (2016). Development of computational model for tunable characteristics of graphene based triangular patch antenna in THz regime. *Journal of Computational Electronics*, 15, 222-227.
  15. Bala, R.; Marwaha, A.; and Marwaha, S. (2016). Performance enhancement of patch antenna in terahertz region using graphene. *Current Nanoscience*, 12(2), 237-243.
  16. Wu, B.; Tuncer, H.M.; Katsounaros, A.; Wu, W.; Cole, M.T.; Ying, K.; Zhang, L.; Milne, W.I.; and Hao, Y. (2014). Microwave absorption and radiation from large-area multilayer CVD graphene. *Carbon*, 77, 814-822.
  17. Dai, Z.; Wang, K.; Li, L.; and Zhang, T. (2013). Synthesis of nitrogen-doped graphene with microwave. *International Journal of Electrochemical Science*, 8, 9384-9389.
  18. Li, C.; Hu, Y.; Yu, M.; Wang, Z.; Zhao, W.; Liu, P.; Tong, Y.; and Lu, X. (2014). Nitrogen doped graphene paper as a highly conductive, and light-weight substrate for flexible supercapacitors. *RSC Advances*, 4(94), 51878-51883.
  19. Wang, Y.; Shao, Y.; Matson, D.W.; Li, J.; and Lin, Y. (2010). Nitrogen-doped graphene and its application in electro-chemical biosensing. *ACS Nano*, 4 (4), 1790-1798.
  20. Rajan, D.S.P. (2019). Design of microstrip patch antenna for wireless application using high performance FR4 substrate. *Advances and Applications in Mathematical Sciences*, 19(1), 53-61.
  21. Bozzi, M.; Pierantoni, L.; and Bellucci, S. (2015). Applications of graphene at microwave frequencies. *Radioengineering*, 24(3), 661-669.
  22. Fu, F.; Xin, S.X.; and Chen, W. (2014). Temperature and frequency-dependent dielectric properties of biological tissues within the temperature and frequency ranges typically used for magnetic resonance imaging-guided focused ultrasound surgery. *International Journal of hyperthermia*, 30(1), 56-65.
  23. Ragab, M.; Abouelregal, A.E.; Alshaibi, H.F.; and Mansouri, R.A. (2021). Heat transfer in biological spherical tissues during hyperthermia of magnetoma. *Biology*, 10(12), 1259.
  24. Gabriel, S.; Lau, R.W.; and Gabriel, C. (1996). The dielectric properties of biological tissues: parametric models for the dielectric spectrum of tissues. *Physics in Medicine and Biology*, 41 (11), 2271-2293.
  25. Trujillo-Romero, C.J.; Salas, L.L.; and Hernandez, A.V. (2011). FEM modeling for performance evaluation of an electromagnetic oncology deep hyperthermia applicator when using monopole, inverted T, and plate antennas. *Progress in Electromagnetics Research*, 120, 99-125.
  26. Bala, R.; Marwaha, A.; and Marwaha, S. (2016). Comparative analysis of zigzag and armchair structures for graphene patch antenna in THz band. *Journal of Materials Science: Materials in Electronics*, 27 (5), 5064-5069.
  27. Gaffoglio, R.; Righero, M.; Giordanengo, G.; Zucchi, M.; and Vecchi, G. (2020). Fast optimization of temperature focusing in hyperthermia treatment of sub-superficial tumors. *IEEE Journal of Electromagnetics, RF and Microwaves in Medicine and Biology*, 5(3), 286-293.

28. Nizam-uddin, N.; and Elshafiey, I. (2017). Enhanced energy localization in hyperthermia treatment based on hybrid electromagnetic and ultrasonic system: proof of concept with numerical simulations. *BioMed Research International*, 2017, 18.
29. Trefná, H.; Vrba, J.; and Persson, M. (2010). Evaluation of a patch antenna applicator for time reversal hyperthermia. *International Journal of Hyperthermia*, 26 (2), 185-197.
30. Fiser, O.; Merunka, I.; and Vrba, J. (2015). Design, evaluation and validation of planar antenna array for breast hyperthermia treatment. *Proceedings of the Conference on Microwave Techniques (COMITE)*, Pardubice, Czech Republic, 1-4.
31. Ling, W.V.; Lias, K.; Buniyamin, N.; Basri, H.M.; and Narihan, M.Z.A. (2021). SAR distribution of non-invasive hyperthermia with microstrip applicators on different breast cancer stages. *Indonesian Journal of Electrical Engineering Computer Science*, 22(1), 232-240.
32. Elsaadi, M.; Aid, Y.; Abbas, M.; Embarek, A.; and Salih, K. (2019). Hyperthermia for breast cancer treatment using slotted circular patch antenna. *Circuits and Systems*, 10 (3), 37-44.